PRAMANA
— journal of
physics

Vol. 75, No. 6
December 2010
pp. 1099–1113

Development of evanescent wave absorbance-based fibre-optic biosensor

T KUNDU[1,*], V V R SAI[2], R DUTTA[1,3], S TITAS[3], P KUMAR[3] and S MUKHERJEE[2]

[1]Department of Physics, Indian Institute of Technology Bombay, Mumbai 400 076, India
[2]Department of Biosciences and Bioengineering, Indian Institute of Technology Bombay, Mumbai 400 076, India
[3]Naval Material Research Laboratory, Mumbai 421 506, India
[*]Corresponding author. E-mail: tkundu@phy.iitb.ac.in

Abstract. Development of chemical and biochemical sensors is the current need of the society. In this report, we present our investigation on the development of a label-free fibre-optic biosensor based on evanescent wave absorbance to detect the presence of analytes such as bacteria, virus and some clinically important proteins. A simple UV-LED (280 nm) and photodetector combination along with a fibre probe was used for developing cost-effective, user-friendly and field applicable device. To improve the sensitivity of the detection technique, the probe design was modified and the U-bent probe was fabricated by simple procedure. Further, to overcome the problems for using UV light source in the fibre, the localized surface plasmon resonance of noble metal nanoparticles at visible wavelength was exploited as a sensing medium for the biochemical reactions. Our systematic studies in this regard presented in this communication may bring the excitement for developing the waterborne pathogen detection device for house-hold as well as field applications.

Keywords. Evanescent wave biosensor; U-bent fibre-optic probe; fibre-optic biosensor; evanescent wave absorbance; gold nanoparticles localized SPR biosensor; silver nanoparticles localized SPR biosensor.

PACS Nos 87.85.fk; 42.79.PW; 42.79.QX

1. Introduction

The presence of waterborne enteric bacteria in municipal water supplies could be a potential human health risk and may lead to death in young children and adults with compromised immune system. These important commodities need to be monitored thoroughly for any presence of pathogenic bacteria or viri. Even though preventive measures for disease outbreak are necessary, because of the recent biothreat, continuous monitoring of surrounding environment such as air, water and food are crucial for timely detection of harmful micro-organisms. Apart from environmental monitoring, clinical diagnosis is important, where technological developments can be aimed at fulfilling the needs of the society.

Several pathogen detection methods are developed and established based on the morphological, cultural, antigenic and genetic characteristics of the organisms [1–4]. These analytical procedures are highly reliable and selective, but the high detection times ranging from few hours to days (colony counting) is a disadvantage. Cost-effective diagnostics, with an ability to diagnose the pathogens instantly and with minimum operating complexities, are necessary. Several detection techniques are developed by incorporating different combinations of biological elements and transduction methods and reviewed [5–10]. Label-free optical biosensors involve detection of analytes in terms of measurement of changes in intensity, peak wavelength, angle of light coupling or phase shift. Sensing phenomena based on evanescent wave absorbance or light scattering, absorbance quenching and autofluorescence depend to a large degree on the optical properties of the analyte under observation, whereas refractive index changes can be obtained by binding of any molecule of significant volume. Optical sensors can be divided into two categories, one that uses the intrinsic properties of a waveguide such as evanescent wave phenomenon for sensing and the other that uses waveguide simply as a light carrier. Most label-free optical detection techniques utilize the evanescent field at the waveguide/biomolecular layer interface to convert the target binding events into optical signal changes. Optical fibres are the simplest form of light waveguides. Ever since their invention, they have been widely used as physical and chemical sensors [11]. Applications of optical fibres in chemical sensing and biosensing are reviewed in detail in [12–19]. For biosensor applications, optical fibres are employed in two configurations; one with biomolecules at the distal end of the fibre probe and other with biomolecules immobilized on the core of the fibre. Thompson and Ligler [20] suggested the use of fluorophores as a means of efficient transduction compared to chromophores due to the higher limits of detection for fluorescence. Thus, most of the biosensor applications of evanescent wave-based fibre-optic sensors were limited to fluorescence-based assays [21,22]. Fibre-optic probe design was optimized to achieve greater evanescent field strength for excitation of fluorophores and maximum coupling of the resultant fluorescence back into the fibre [23]. There are several reports on evanescent wave absorption spectroscopy using fibre-optics in visible and near infra-red spectral regions [24]. Paul and Kychakoff [25] observed that the evanescent power and hence absorbance is inversely proportional to V, where V is the normalized frequency parameter. An expression for evanescent absorbance is derived in terms of evanescent power ratio, bulk coefficient and length of the probe on the basis of a pseudo-Beer's law relationship [26,27]. Some researchers attempted to improve evanescent power by adopting coiled [26], bent [28,29] and tapered [30] fibres. Some of the widely explored transduction techniques capable of detecting RI changes in microenvironment on the sensor surface include SPR [31,32], localized SPR (LSPR) [33], interferometry [34], grating couplers [35], photonic crystal biosensors [36] and photonic band gap biosensors [37].

In this report, we outline the feasibility of developing an evanescent wave absorbance (EWA) based fibre-optic biosensor by exploiting the absorbance properties of either the analytes or the sensing medium. Recently, we have demonstrated the possibility of immunodetection of biomolecules such as IgG using evanescent wave absorbance from straight fibre-optic probes at 280 nm wavelength [38]. Similarly, optical absorbance properties of proteins associated with pathogens at 280 nm

wavelength can be exploited to develop a biosensor with better sensitivity. Straight fibre-optic probes, however, suffer from low penetration depth of evanescent field (effective distance typically $<\lambda/10$) particularly for UV region. Thus, they are unsuitable for larger analytes such as bacteria. This problem can be addressed by adapting optical fibre probes with modified geometry that are capable of improving the evanescent field intensity and/or its penetration depth [16]. Amongst several fibre-optic probe designs, U-bent optical fibre probes are more attractive and feasible because of simpler probe design and fabrication [28,39]. On the other hand, absorption of UV light by the core of the silica optical fibre limits its wide use for pathogen detection. Refractive index changes taking place at the surface of the nanoparticles result in changes in plasmonic absorbance in the visible region and a red shift in absorbance peak. These properties of Au and Ag nanoparticles were utilized in liquid phase as well as monolayers coated on glass/quartz substrates to develop colorimetric biosensors [40–44]. Our group addressed these problems and realized the potential of U-bent fibre-optic probes in absorbance-based detection of analytes, especially of larger size (>40 nm) and developed a sensitive EWA-based localized surface plasmon resonance (LSPR) biosensor [45]. Here, we describe the systematic development of these evanescent wave absorbance-based biosensor using fibre-optic probes.

2. Theoretical background

Evanescent absorbance in the optical fibre can be expressed in terms of evanescent power ratio, bulk coefficient and length of the probe on the basis of a pseudo-Beer's law relationship [25–27].

The optical power transmitted by an optical fibre decladded for a portion of length L is given by

$$P(L) = P(0)\mathrm{e}^{-\alpha L}, \tag{1}$$

where $P(0)$ is the initial optical power launched into the fibre, α is the evanescent absorption coefficient and L is the length of the decladded fibre. Evanescent absorbance, A, is given by

$$A = \frac{P_{\mathrm{clad}}}{P(0)}\frac{\beta L}{2.303}, \tag{2}$$

where β is the absorption coefficient and (P_{clad}/P) can be termed as optical power ratio, P_{clad} is the evanescent wave optical power at the surface of the cladding and $P(0)$ is the total power coupled into fibre. Optical power ratio is inversely proportional to the total number of modes that can exist in the waveguide. It can be replaced by an expression in terms of known waveguide parameters [27] as shown below.

$$A = k\frac{\sqrt{2}\times 4\lambda}{3\times 2\pi r NA}\varepsilon_{\mathrm{ex}} cL, \tag{3}$$

where r is the radius of the optical fibre into which light is coupled, NA is the numerical aperture at the sensing region of the fibre, λ is the wavelength of light,

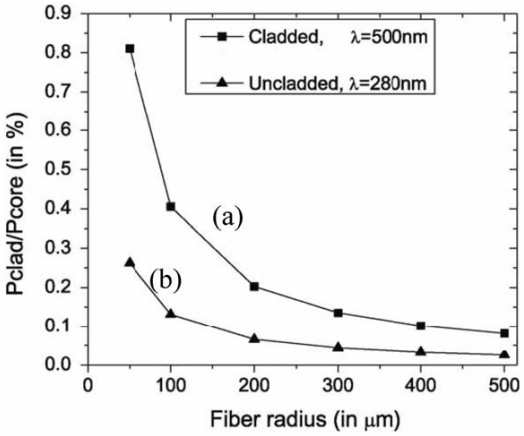

Figure 1. Effect of optical fibre radius on the optical power ratio between the evanescent field at the cladding and core in different operating conditions. (**a**) The optical fibre with NA = 0.37 is cladded (-■-); (**b**) the fibre is decladded and surrounded by aqueous medium (refractive index = 1.35052) at 280 nm as in the case of biomolecules and bacterial cell detection (-▲-).

ε_{ex} is the extinction coefficient of the absorbing medium and c is the concentration of the absorbent molecules bound per unit circumferential surface area of the fibre. Here k is a correction factor in order to take the upper limit for the presence of chromophores around the fibre core into consideration. Figure 1 presents effects of optical fibre radius on the ratio of the optical power in the cladding and the core for given values of numerical aperture and wavelength. It is evident from figure 1 and eq. (3) that the changes in the optical power ratio, and hence the evanescent absorbance of the sensor improves by choosing fibres of smaller diameter and by achieving lower numerical aperture.

3. Experimental methods

3.1 *Reagents and materials*

Tetrachloro aurate ($HAuCl_4$), cystamine ($HS–C_2H_4–NH_2$) and phosphate buffer saline (PBS) were obtained from Sigma. Aminosilane (N-[3-trimethoxy silyl]propyl) ethylene diamine, >99%) was procured from Aldrich. Glutaraldehyde ($OHC–C_2H_4–CHO$) was obtained from Fluka. Trisodium citrate and acetic acid were purchased from SD Fine Chemicals, India. All antibodies, human IgG (HIgG), rabbit IgG (RIgG) and goat anti-human IgG-affinity purified (GaHIgG) and bovine serum albumin (BSA) were obtained from Bangalore Genei, India. All the reagents were of analytical grade. $AgNO_3$ (99.8%) was obtained from Dhawal Chemical Reagent Co., Ltd. $NaBH_4$ (96.0%) was procured from Sinopharm Chemical Reagent Co., Ltd. Trisodium citrate and acetic acid were obtained from SD Fine Chemicals,

India. All solutions were prepared using de-ionized (DI) water obtained from a MilliQ filtration system. Optical fibres were procured from Thorlabs®.

3.2 *Fibre probe preparation*

The fibres were cut into 40 cm long pieces. Typically, 2–5 cm length in the middle of the fibre was decladded to expose its core. The buffer and cladding were stripped by using a sharp surgical blade. The terminal ends of the optical fibre were polished using emery papers with 5, 1 and 0.3 μm roughness in sequential order.

Silica fibre probes were treated with sulphochromic solution (2.5 mg $K_2Cr_2O_7$ +1 ml of DI water + 100 ml conc. H_2SO_4) for 8–10 min to generate hydroxyl groups on the surface resulting in the formation of silanol (Si–OH) sites on the surface. Subsequently, the surfaces were thoroughly washed twice in DI water. Fibres were placed in a hot air oven and dehydrated at 115°C for 2 h.

For aminosilanization, fibre probes were removed from the oven and dipped in 1% silane prepared in absolute ethanol for 3–5 min in argon ambient. The pH of the solution was maintained at 3.7 so as to keep the amino terminals away from the anionic silanol surface [36]. Probes were washed in absolute ethanol after treatment with silane. The fibres were subsequently heated to 110°C in argon ambient to allow condensation of the silanols from the aminosilane and the surface forming siloxane bonds. This lends greater stability and is a crucial step in the process. For glutaraldehyde treatment, aminosilanized surfaces were treated in 1% glutaraldehyde, a homobifunctional crosslinker, prepared in DI water. After 30 min, substrates were washed in DI water. Amine functional groups react with the aldehyde groups at one end of glutaraldehyde forming imine bonds, leaving aldehyde groups at the other end to react with the antibody.

For antibody immobilization, the sensor region of each fibre was incubated in 0.1 mg/ml of human IgG antibody solution prepared in PBS of 7.4 pH for overnight. After 12 h, the probes were washed in PBS thoroughly to remove any loosely adsorbed molecules.

We attempted bending of 200 μm diameter fibres using a simple wax candle flame [38]. The bluish flame at the bottom of the flame was used to obtain 0.5–1 mm radius. The bent portions were observed under an optical microscope and diameters were measured from the images of U-bent probes by using Axiovision® software (Carl-Zeiss®). The core diameter of the fibre was found to be uniform at the bent portion.

3.3 *Optical set-up*

The optical set-up for absorbance measurements consists of a xenon lamp with spectral emission between 350 and 800 nm or a UV-LED (T9H28C from Roithner Lasertechnik GmbH, Austria) with peak emission at 280 nm and a fibre spectrometer. One of the polished ends of the prepared fibre sensor probe was held by a fibre chuck in fibre coupler (Newport®, USA). Light from xenon lamp or UV-LED was focussed through a microscopic objective lens, 40×, 0.4 NA, onto the fibre

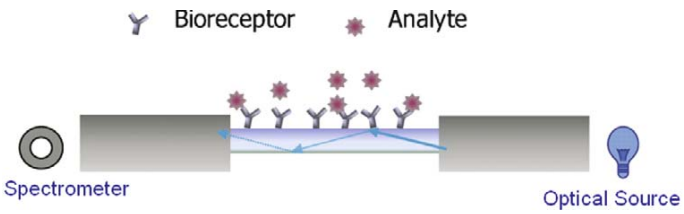

Figure 2. Schematic of sensing protocol for evanescent wave absorbance measurement from a fibre-optic probe with the help of an optical source and fibre-optic spectrometer.

end. The decladded fibre sensor portion was held within a glass capillary tube with inlet and outlet ports. The other end of the fibre was held by using a fibre positioner. Light from this end was collected into a fibre-optic spectrometer (S 2000, Ocean Optics). Binding events taking place on the fibre probe surface were monitored as absorbance changes in real-time and the full absorbance spectra were also recorded. OO1Base32 software was used for obtaining absorbance spectra. Signal-to-noise ratio (SNR) was improved by averaging 100 consecutive spectra. A schematic diagram of the typical experimental set-up is given in figure 2.

3.4.1 *Synthesis of gold nanoparticles.* Gold nanoparticles used in these experiments were synthesized using the procedure described by Turkevich *et al* [46]. 50 mM $HAuCl_4{\cdot}3H_2O$ in DI water was prepared as a stock solution. 0.2 ml of 50 mM gold chloride solution was added to 39.15 ml of DI water and heated until it began to boil. 0.647 ml of 5 mg/mL sodium citrate trihydrate solution was added as soon as boiling commenced. Heating was continued until the solution turned pale purple. Then the solution was removed from the hot plate and allowed to cool to room temperature. The molar ratio of citrate to gold was 1:1. The average size of the synthesized nanoparticles was 40 nm. The absorbance peak for gold nanoparticles in solution was at 530 nm.

3.4.2 *Synthesis of silver nanoparticles.* Silver nanoparticles used in these experiments were prepared by adding $NaBH_4$ solution drop by drop (7.2 mM, 1.0 ml) to an aqueous solution of $AgNO_3$ (0.09 mM, 100 ml) in the presence of sodium citrate (0.081 mM) under vigorous stirring [47]. The stirring process was continued for 30 s more after adding $NaBH_4$. The solution turned light-greenish yellow. Resulting solution has a pH of 7. The average size of the synthesized nanoparticles was around 30 nm. The absorbance peak for silver nanoparticles in solution was at 396 nm.

4. Results and discussions

4.1 *Response of straight silanized fibre*

Each silanized straight fibre probe (5 cm long) was loaded into a capillary tube and white light was coupled into one of its two ends and captured at the other

end through a lens into an optical fibre coupled to a spectrometer. Fluorescein isothiocyanate (FITC) in borate buffer, 0.1 mM was injected into the capillary tube, silanized fibre probes of different diameters were subjected to FITC for 15 min and absorbance was measured after washing the unbound molecules.

The absorption spectra of FITC molecules through the fibre probes of different diameters are given in figure 3. Though the absorption spectrum from the probes was expected to be almost the same as free FITC molecules, a red-shift in the peak absorbance from 494 to 500 nm was observed. The absorbance values were found to rise with decrease in the fibre diameter as expected from eq. (3). Clean bare fibre probes were also tested with FITC solution. The absorbance of bare fibre at 500 nm (A500nm) in the presence of 0.1 mM FITC was nearly 0.015, as shown in figure 3. No significant absorbance however, was observed after FITC molecules in the capillary tube around the fibre probes were washed with borate buffer because the amine functional groups necessary for FITC binding were absent on fibre surface. The fact that no significant absorbance was noticed with these fibres proved that the evanescent wave phenomenon was confined to the surface and its close proximity. It can be concluded that molecules (analytes) that are not bound to the surface will have negligible effect on absorbance. HIgG immobilized, 5 cm long, 200 μm fibre probes were tested by incubating the samples in 0.05 mg/ml of FITC-tagged GaHIgG antibodies for 20 min. The number of target analyte molecules binding to the immobilized bioreceptors is known to reach saturation for the above concentration and incubation time. The saturated value of A500nm obtained because of the presence of FITC tagged GaHIgG on the sensor surface was observed to be 0.04. Hence, 200 μm, 5 cm long fibre probe was able to detect the presence 0.05 mg/ml of the target analyte.

With the proof of the concept for EWA at 500 nm, we tried to understand the efficiency of these probes in detecting various concentrations of anti-IgG and

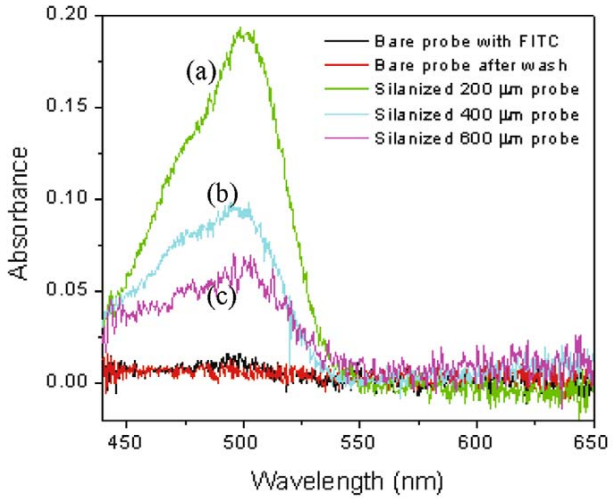

Figure 3. Absorbance spectra of FITC obtained from silanized fibre probes of (**a**) 200 μm, (**b**) 400 μm and (**c**) 600 μm core diameters.

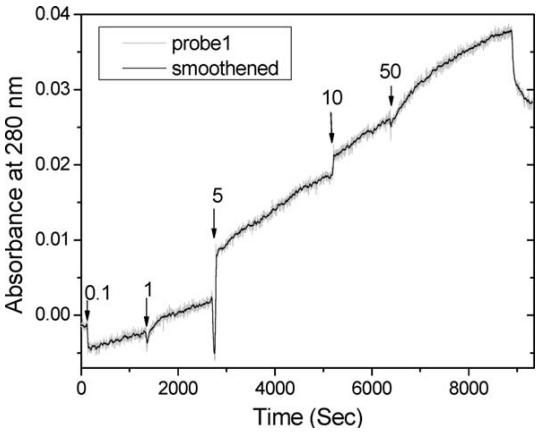

Figure 4. Time-resolved absorbance response of HIgG immobilized probes when incubated for different concentrations (μg/ml) of GaHIgG biomolecules. Note: the abrupt changes in absorbance are because of the disturbances caused during the introduction of analyte into flow channel containing fibre probe.

minimum detection limit. 5 cm long, 200 μm fibre sensor probes were silanized and incubated with 0.1 mg/ml HIgG solution for 16 h to immobilize bioreceptors on the fibre core. These probes were used to obtain absolute absorbance at various concentrations of GaHIgG and the corresponding time-resolved response. These probes were subjected to sequentially higher concentrations of the analyte. Figure 4 shows time-resolved response at 280 nm obtained by subjecting these probes to a wide range of analyte concentrations from 0.1 to 50 μg/ml prepared in 5 mg/ml BSA solution. The initial drop in absorbance was due to refractive index changes between PBS and 5 mg/ml BSA in PBS (1.3347 and 1.3335). When a probe was subjected to 0.1 μg/ml of GaHIgG, a rise in absorbance was observed with a change of 0.0025 after 20 min. The change in the absorbance value at 280 nm to the maximum concentration of GaHIgG (50 μg/ml) was obtained as 0.036.

These studies have shown that the development of evanescent wave absorbance-based label-free fibre-optic biosensor for detecting biomolecules utilizing their inherent optical absorbance properties is possible. But, experiments with straight fibre probes for detecting *E. Coli* bacterial cells resulted in poor absorbance changes because of the weak evanescent field and small penetration depth of the evanescent wave.

4.2 *Response of U-bent fibre*

The depth of penetration, d_{p}, of the evanescence wave is defined as the distance at which the magnitude of the electric field at the surface decays to its $1/e$ value and given by

$$d_{\mathrm{p}} = \frac{\lambda}{2\pi n_{\mathrm{co}}\sqrt{(\sin^2\theta - (n_{\mathrm{cd}}^2/n_{\mathrm{co}}^2))}}, \tag{4}$$

where n_{co} and n_{cd} are the refractive indices of the core and cladding of the fibre and θ is the internal incident ray angle with the normal to the core/cladding interface. As the wavelength of light λ decreases (towards the UV region), the penetration depth decreases.

Different geometric designs for fibre-optic probes have been proposed for different applications. These designs were aimed at improving the optical power ratio and depth of penetration at the surface of the fibre core by means of tapering [30], coiling [26] or bending [28,29] the fibre core. Among these, U-bent probes have distinct advantages such as, high penetration depth, ease of fabrication and ease of handling. Although the response of U-bent probes is influenced only by its bend radius, optimum designs have already been reported for specific applications [39,48]. The evanescent field at the bent portion of a 200 μm core diameter U-probe may vary from 300 to 600 nm at a wavelength of 632 nm. Hence, sensing of bacterial cells and viri that occupy a space up to 50–500 nm from the core/cladding interface may elicit better absorption response as opposed to simple proteins that lie within 20 nm from the fibre core [48].

To test the U-bent probes with bacterial cells, a bend probe (figure 5a) with a diameter of 1.05 mm was functionalized and immobilized with antibodies to *E. coli* cells. 15×10^2 cells/ml were introduced into the capillary tube and absorbance changes at 274 nm were observed due to binding of *E. coli* cells to probe. Response was monitored till the saturation and higher concentration of cells was introduced as shown in figure 5b. It was observed that the change in absorbance due to binding of *E. coli* cells on U-bent fibre was one order of magnitude higher than the straight fibre with the same concentration of *E. coli* cells. This experiment clearly demonstrates the improvements in the absorbance sensitivity to *E. coli* cells by using U-bent probes. It was however, observed that the sensor performance for small concentration of *E. coli* cells was limited by the number of cells near U-bent region. Hence, sensor performance in this kind of methodology could be improved by injecting sample solution at a constant flow rate and also by reducing the liquid volume around the probe.

In these kinds of sensors, absorption of UV lights (280 nm) by the fibre core (silica) itself limits its exploitation as an effective biological sensor. The penetration depth in a UV region is also lesser than in the visible and IR regions (figure 1). To overcome this problem, metal nanoparticle can be exploited as sensing medium. Nanoparticles of noble metals such as gold and silver exhibit optical absorption and scattering properties in UV–visible region termed as localized surface plasmon resonance (LSPR) [49]. The extinction band due to LSPR is influenced by the size, shape and composition of nanoparticles and most importantly by the surrounding environment [40–43].

4.3 *Response of LSPR-based fibre*

In surface plasmon resonance, light interacts with particles much smaller than the incident wavelength. This leads to a plasmon that oscillates locally around the nanoparticle with a frequency known as the localized surface plasmon resonance (LSPR). According to Mie's theory, the dipolar absorption efficiency (Q_{abs}) of a

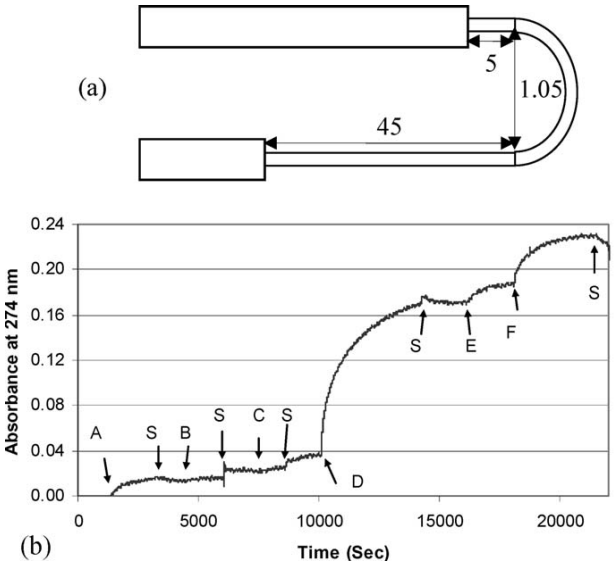

Figure 5. Time-resolved absorbance response at 274 nm of a U-bent probe (**a**) of diameter ∼1 mm with *E. Coli* cell count and (**b**) 15×10^2 (A), 15×10^3 (B), 15×10^4 (C), 15×10^5 (D), 15×10^6 (E), 15×10^7 (F) and saline (S) respectively.

single metal sphere with radius R is given by [50]

$$Q_{\text{abs}} = \frac{24\pi R}{\lambda} \frac{\varepsilon_m^{3/2}\varepsilon''(\omega)}{(\varepsilon'(\omega) + G\varepsilon_m)^2 + (\varepsilon''(\omega))^2}, \tag{5}$$

where $\varepsilon'(\omega)$ and $\varepsilon''(\omega)$ are the real and imaginary parts of the dielectric constant of a metal of wavelength, $\lambda(= 2\pi c/\omega)$. ε_m is the dielectric constant of external environment. R and G are the size and shape factor of the metal nanoparticle, respectively. The value of G is 2 for a spherical nanoparticle, but it takes on values as large as 20 to account for particle geometries with high aspect ratios. From the equation, it is also obvious that extinction would be maximum when $\varepsilon'(\omega) + 2\varepsilon_m = 0$ and this gives rise to strong resonance band. Thus, it is clear that this surface plasmon resonance would be sensitive to the dielectric constant of external environment ε_m. Using this methodology, gold and silver nanoparticles-based sensors were studied.

4.3.1 *Gold nanoparticles-based fibre probes.* Gold nanoparticles (GNP) were bound to amine functionalized U-bent fibre probes as described below. A silanized U-bent sensor probe with a bend radius of 0.75 mm was positioned between the source and detector with the bend region of the sensor probe in a custom-made glass capillary of 2.5 mm diameter. The capillary tube was used to incubate the probe with GNP solution and also to subject the probes to solutions with different refractive indices at later stages of the experiments. The GNP solution was introduced into the capillary tube and absorbance spectrum was monitored in real-time. The peak

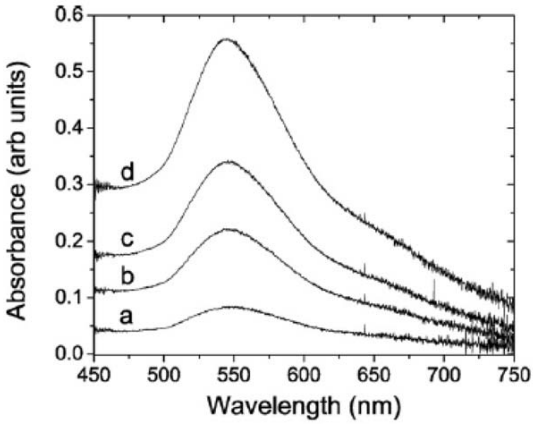

Figure 6. Absorbance spectra of bind gold nanoparticles on fibre obtained for sucrose solutions with refractive index values (**a**) 1.3359, (**b**) 1.3403, (**c**) 1.3433 and (**d**) 1.3494.

absorbance of the spectrum reached nearly three units within a time span of 30–60 min of incubation. Above an absorbance of about 2.5–3 units, the high absorption of light at the peak absorption wavelength of GNP gave rise to a noisy signal. The absorbance spectrum recorded from the probe is shown in figure 6. The spectral characteristics of GNP-coated fibres were slightly different from that of GNP in solution phase. A red-shift in the peak wavelength and a broadening of the spectrum was noticed in the spectrum. Further, a plateau centred at 650 nm was observed in the spectrum. The red-shift in the peak wavelength was observed from the beginning of the deposition of GNP onto the sensor probe. An average red-shift of 13.4 ± 1.4 nm was observed. In fact, the occurrence of red-shift may be due to plasmon coupling between the chemisorbed GNP with an interparticle distance less than $\sim$2.5 times the particle size [51,52]. The plateau, observed at 650 nm in addition to the red-shift, may have resulted from aggregation of GNP due to higher surface roughness of aminosilane layer on fibre and/or the size distribution of nanoparticles [41,44,53]. Subsequently, GNP-coated probes were used for testing the bulk refractive index sensitivity.

Sucrose solutions of different concentrations with refractive indices between 1.33 and 1.40 were introduced and absorbance response was recorded. Figure 6 shows the absorbance spectra obtained by subjecting the GNP-coated sensor probe with consecutively higher % (w/w) sucrose solutions with RI varying from 1.33 to 1.35. A significant rise in absorbance was obtained for different RI solutions. But, no significant shift in peak wavelength was observed. Bare U-bent probes are known to be sensitive to refractive index. In order to investigate the contribution of bending alone in the absorbance response, a bare bent probe of 0.5 mm radius and later the same probe coated with GNP were subjected to RI variation between 1.33 and 1.40 and absorbance response at 540 nm was monitored. The bare probe was found to induce a change in absorbance that was approximately one tenth of the absorbance obtained in the presence of GNP monolayer. An important observation was the limitation of range of the RI detection between 1.33 and 1.38 RIU in

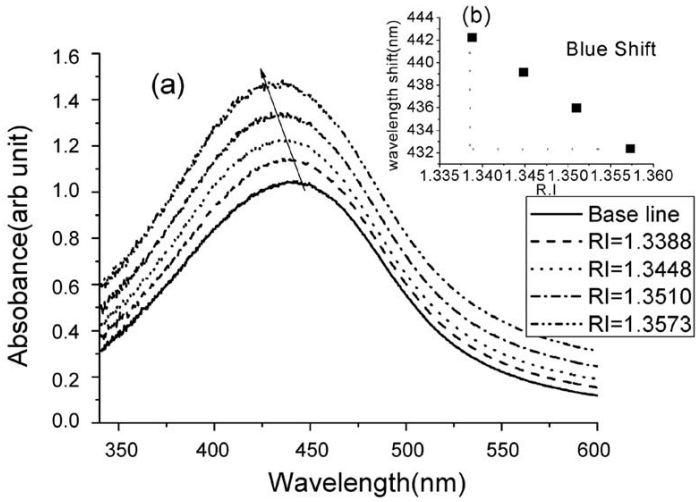

Figure 7. Absorbance spectra of bind silver nanoparticles on the fibre obtained for sucrose solutions with refractive index values 1.3388 to 1.3573.

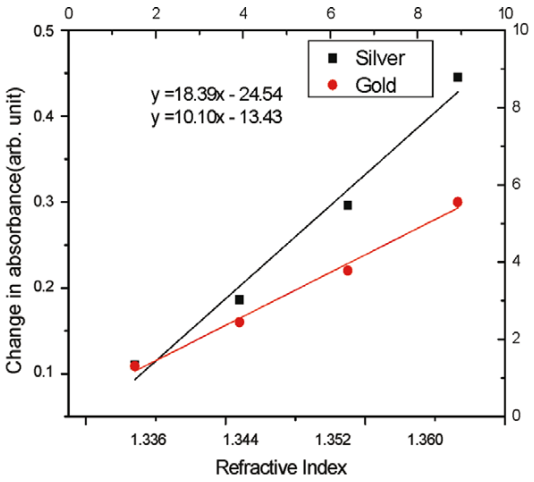

Figure 8. Response of the change in absorbance for silver and gold nanoparticles due to different refractive indices of the medium. The initial absolute absorbance at 1.3388 was 1 for both the cases.

aqueous phase. Effective light coupling between U-bent probe and GNP as well as significant absorption of light in the presence of high RI solutions led to peak absorbance values of more than 2.5 units for RI of above 1.38. This resulted in poor signal-to-noise ratio. Sensitivity was found to be influenced by the bend radius of the probe with its value of 28.98 and 35.19 A540nm/RIU for 0.5 and 0.75 mm probes respectively [45].

4.3.2 *Silver nanoparticles-based fibre probes.* The silanized optical fibre was incubated in the silver nanoparticle (AgNP) solution and the absorption spectrum was taken at definite time intervals. In this case also, it was observed that the resonance peak was shifted towards the red side of the spectrum when these Ag nanoparticles were attached to the core surface of the fibre. The absorption peak then increased as well monotonously shifted to the red side further with time. With the increase in incubation time, the number of AgNP per unit area of the surface, i.e. particle surface concentration increased, which introduced red-shift as well as intensity change. After the incubation of the nanoparticles, the effect of the environment dielectric medium was also carried out. It was observed that with the increase in refractive index of the medium from 1.33 to 1.3573, the plasmon resonance peak was shifted to blue side of the spectrum as shown in figure 7. Along with the blue-shift, the intensity of the resonance peak also increased. This change in intensity is presented in figure 8. In this figure, the intensity change of the gold nanoparticles is presented for comparison. It was observed that the rate of intensity change in AgNP is higher than that of GNP with the same refractive index change ($\Delta A/\Delta RIU$ for AgNP is 18.4 and for GNP is 10.1). This is attributed to the smaller bandwidth of the absorption spectrum of AgNP than that of GNP. Thus, AgNP-based sensor might show higher sensitivity than the GNP-based sensors.

5. Conclusion

Our studies have shown that the development of evanescent wave absorbance-based label-free fibre-optic biosensor for detecting biomolecules utilizing their inherent optical absorbance properties is possible. Advantages of the EWA-based fibre-optic biosensors include promising sensitivity, low interference of visible light in sensing and simple immobilization chemistry. The fibre-optic probes are cost-effective, easy to fabricate and easy to use. Experiments with straight fibre probes for detecting *E. Coli* bacterial cells resulted in poor absorbance changes. Apart from the instrumentation development point of view, the disadvantages include the cost of UV-LED and photodetector and high electrostatic sensitivity of these optical components. In fact, UV light technology is yet to mature to produce affordable UV laser diodes operating at 280 nm. Further, most photodetectors operating in the UV region are also limited by small values of spectral responsivity compared to visible and NIR photodetectors. Thus, efficient optical detection at 280 nm could be another drawback. The sensor performance may be improved using smaller fibre diameter and/or larger probe lengths. But, thinner and longer probes may be fragile and more difficult to handle. These limitations due to weak evanescent field and small penetration depth values in UV region may be overcome by modifying geometric design of the sensor probe. U-bent fibre probes possess relatively higher penetration depth and hence have potential applications in realizing EWA-based biosensors for bacteria and virii. In a separate study carried out in our group, experiments with U-bent probes for detecting *E. Coli* cells have shown promising results [54]. Recently, we have developed efficient absorbance biosensors using U-bent fibre probes based on localized surface plasmon resonance (LSPR) [45]. They are capable of detecting bulk refractive index changes with a sensitivity and resolution of 35.19 A540nm/RIU and 3.8×10^{-5} RIU respectively. Apart from issues

related to probe design, it is also true that for such sensors the performance is limited by the extinction coefficient of the target analyte and hence its molecular weight. As a result, EWA-based biosensors may not be sensitive to analytes with a molecular weight less than 1 kDa. In addition, detection of analytes of larger volume such as whole cells and very large molecules may be limited by low evanescent field strength and smaller penetration depths compared to the size of the analytes. In other words, a significant portion of the bound cells do not come under the influence of the evanescent field. In conclusion, these sensors have promising potential for various applications in different fields.

Acknowledgement

The authors thank Naval Material Research Laboratory (NMRL), Ambernath, for funding this research.

References

[1] J M Pelczar, E C S Chan and N R Krieg, *Microbiology* (McGraw-Hill, New York, 1986)
[2] I L Pepper, C P Gerba and J W Brendecke, *Environmental microbiology – A laboratory manual* (Academic Press, San Diego, CA, 1995) pp. 67–127
[3] J P Duguid, B P Marmion and R H Swain, *Mackie and McCartney medical microbiology* (ELBS/Churchill Livingstone, Edinburgh, 1978) Vol. 1
[4] L M Prescott, J P Harley and D A Klein, *Microbiology* (WCB McGraw-Hill, 1999) Chap. 2, 15, 32, 41
[5] K Kerman Kobayashi and E Tamiya, *Meas. Sci. Technol.* **15**, R1 (2004)
[6] C L Morgan, D J Newman and C P Price, *Clin. Chem.* **42(2)**, 193 (1996)
[7] R C McGlennen, *Clin. Chem.* **47(3)**, 393 (2001)
[8] N L Rosi and C A Mirkin, *Chem. Rev.* **105**, 1547 (2005)
[9] K K Jain, *Clin. Chim. Acta* **358**, 37 (2005)
[10] M A Cooper, *Anal. Bioanal. Chem.* **377**, 834 (2003)
[11] D A Krohn, *Fiber optic sensors: Fundamentals and applications* (Instrument Society of America, 1992) Second edition
[12] O S Wolfbeis, *Fiber optic chemical sensors and biosensors* (CRC Press, Boca Raton, 1991) Vols 1 & 2
[13] O S Wolfbeis, *Fiber-optic chemical sensors and biosensors, bi-annual reviews from 2000 to 2008, Anal. Chem.* **72(12)**, 81 (2000); **74(12)**, 2663 (2002); **76(12)**, 3269 (2004); **78(12)**, 3859 (2006); **80(12)**, 4269 (2008)
[14] M D Marazuela and M C Moren-Bondi, *Anal. Bioanal. Chem.* **372**, 664 (2002)
[15] M E Bosch, A J R Sánchez, F S Rojas and C B Ojeda, *Sensors* **7**, 797 (2007)
[16] A Leung, P M Shankar and R Mutharasan, *Sens. Actuators B: Chemical* **125**, 688 (2007)
[17] A Leung, P M Shankar and R Mutharasan, *Sens. Actuators* **B131(2)**, 640 (2008)
[18] A Leung, P M Shankar and R Mutharasan, *Sens. Actuators* **B129**, 716 (2008)
[19] A Leung, P M Shankar and R Mutharasan, *Sens. Actuators* **B123**, 888 (2007)
[20] R B Thompson and F S Ligler, *Biosensors with fiber optics* (Wise and Wingard, The Humana Press, 1991) p. 111
[21] N Nath, S R Jain and S Anand, *Biosens. & Bioelectron.* **12(6)**, 491 (1997)

[22] C R Taitt, G P Anderson and F S Ligler, *Biosensors & Bioelectronics* **20**, 2470 (2005)
[23] G P Anderson, J P Golden, L K Cao, D Wijesuriya, L C Shriver-lake and F S Ligler, *IEEE Eng. Med. Biol.* **13(3)**, 358 (1994)
[24] G J Muller, *Multichannel image detectors* edited by J Talmi (American Chemical Society, New York, 1979) p. 241
[25] P H Paul and G Kychakoff, *Appl. Phys. Lett.* **51**, 12 (1987)
[26] M D DeGrandpre and L W Burgess, *Anal. Chem.* **60**, 2582 (1988)
[27] V Ruddy, B D MacCraith and J A Murphy, *J. Appl. Phys.* **67(10)**, 6070 (1990)
[28] B D Gupta, H Dodeja and A K Tomar, *Opt. Quantum Electron.* **28**, 1629 (1996)
[29] D Littlejohn, D Lucas and L Han, *Appl. Spectrosc.* **53(7)**, 845 (1999)
[30] A G Mignani, R Falciai and L Ciaccheri, *Appl. Spectros.* **52**, 546 (1998)
[31] J Homola (Ed.), *Surface plasmon resonance based sensors* (Springer-Verlag, Berlin, Heidelberg, 2006)
[32] J Homola, *Chem. Rev.* **108**, 462 (2008)
[33] D K Kim, K Kerman, M Saito, R R Sathuluri, T Endo, S Yamamura, Y S Kwon and E Tamiya, *Anal. Chem.* **79(5)**, 1855 (2007)
[34] B Y Shew, C H Kuo, Y C Huang and Y H Tsai, *Sens. Actuators A Phys.* **120(2)**, 383 (2005)
[35] K Schmitt, K Oehse, G Sulz and C Hoffmann, *Sensors* **8**, 711 (2008)
[36] C J Choi and B Cunningham, *Lab. Chip.* **6**, 1373 (2006)
[37] H Ouyang, L A DeLouise, B J Miller and P M Fauchet, *Anal. Chem.* **79(4)**, 1502 (2007)
[38] V V R Sai, T Kundu, C Deshmukh, S Titus, P Kumar and S Mukherji, *Sens. Actuators* **B143(2)**, 724 (2010)
[39] S K Khijwania and B D Gupta, *Opt. Commun.* **175**, 135 (2000)
[40] P Englebienne, *Analyst* **123**, 1599 (1998)
[41] K C Grabar, R G Freeman, M B Hommer and M J Natan, *Anal. Chem.* **67**, 735 (1995)
[42] N Nath and A Chilkoti, *Anal. Chem.* **74**, 504 (2002)
[43] H-Y Lin, C-T Chen and Y-C Chen, *Anal. Chem.* **78**, 6873 (2006)
[44] F Frederix, J-M Friedt, K-H Choi, W Laureyn, A Campitelli, D Mondelaers, G Maes and G Borghs, *Anal. Chem.* **75**, 6894 (2003)
[45] V V R Sai, T Kundu and S Mukherji, *Biosens. Bioelectron.* **24(9)**, 2804 (2009)
[46] J Turkevich, P C Stevenson and J Hiller, *Discuss. Faraday Soc.* **11**, 55 (1951)
[47] B Tang, S Xu, J An, B Zhao and W Xu, *J. Phys. Chem.* **C113**, 7025 (2009)
[48] S K Khijwania and B D Gupta, *Opt. Commun.* **152**, 259 (1998)
[49] K K Jain, *Clin. Chim. Acta* **358**, 37 (2005)
[50] Katherine A Willets and Richard P Van Duyne, *Annu. Rev. Phys. Chem.* **58**, 267 (2007)
[51] T Jensen, L Kelly, A Lazarides and G C Schatz, *J. Cluster Sci.* **10**, 295 (1999)
[52] K H Su, Q H Wei, X Zhang, J J Mock, D R Smith and S Schultz, *Nano Lett.* **3**, 1087 (2003)
[53] G Bar, S Rubin, R W Cutts, T N Taylor and T A Zawodzinski, *Langmuir* **12**, 1172 (1996)
[54] R Bharadwaj, V V R Sai, K Thakare, A Dhawangale, T Kundu, S Titus, P Kumar Verma and S Mukherji (communicated for publication)